

Estuarine plastisphere as an overlooked source of N₂O production

Xiaoxuan Su^{1,2,12}, Leyang Yang^{1,3,12}, Kai Yang ¹, Yijia Tang ⁴, Teng Wen⁵, Yingmu Wang⁶, Matthias C. Rillig^{7,8}, Lena Rohe⁹, Junliang Pan ¹⁰, Hu Li¹ & Yong-guan Zhu ^{1,3,11}✉

“Plastisphere”, microbial communities colonizing plastic debris, has sparked global concern for marine ecosystems. Microbiome inhabiting this novel human-made niche has been increasingly characterized; however, whether the plastisphere holds crucial roles in biogeochemical cycling remains largely unknown. Here we evaluate the potential of plastisphere in biotic and abiotic denitrification and nitrous oxide (N₂O) production in estuaries. Biofilm formation provides anoxic conditions favoring denitrifiers. Comparing with surrounding bulk water, plastisphere exhibits a higher denitrifying activity and N₂O production, suggesting an overlooked N₂O source. Regardless of plastisphere and bulk water, bacterial and fungal denitrifications are the main regulators for N₂O production instead of chemodenitrification. However, the contributions of bacteria and fungi in the plastisphere are different from those in bulk water, indicating a distinct N₂O production pattern in the plastisphere. These findings pinpoint plastisphere as a N₂O source, and provide insights into roles of the new biotope in biogeochemical cycling in the Anthropocene.

¹Key Laboratory of Urban Environment and Health, Institute of Urban Environment, Chinese Academy of Sciences, 1799 Jimei Road, 361021 Xiamen, China. ²Interdisciplinary Research Center for Agriculture Green Development in Yangtze River Basin, College of Resources and Environment, Southwest University, 400715 Chongqing, China. ³University of the Chinese Academy of Sciences, 100049 Beijing, China. ⁴School of Life and Environmental Sciences, The University of Sydney, Sydney, NSW 2015, Australia. ⁵School of Geography, Nanjing Normal University, 210023 Nanjing, China. ⁶College of Civil Engineering, Fuzhou University, 350116 Fuzhou, China. ⁷Freie Universität Berlin, Institute of Biology, Berlin, Germany. ⁸Berlin-Brandenburg Institute of Advanced Biodiversity Research, Berlin, Germany. ⁹Thünen Institute of Climate-Smart Agriculture, Bundesallee 65, Berlin, Germany. ¹⁰School of Electrical Engineering, Chongqing University, 400044 Chongqing, China. ¹¹State Key Laboratory of Urban and Regional Ecology, Research Center for Eco-Environmental Sciences, Chinese Academy of Sciences, 100085 Beijing, China. ¹²These authors contributed equally: Xiaoxuan Su, Leyang Yang. ✉email: ygzhu@rcees.ac.cn

Plastic debris is ubiquitous and problematic in global marine ecosystems^{1–3}. With the increasing public perception of plastic pollution, increasing research efforts have been devoted to revealing the impacts of plastic debris on fish⁴, invertebrates⁵, sea birds⁶, turtles⁷, and microorganisms⁸ in oceans. In recent years, these buoyant plastic debris pieces in marine environments have been reported to provide durable substrates for microorganisms, facilitating colonization and biofilm formation^{9,10}. Microbial communities on plastic debris have been called “plastisphere” and represent a novel feature in the Anthropocene, even sometimes called the eighth continent, sparking global interest^{9–14}. Recent studies have shown that plastisphere exhibited great differences in microbial community and assembly from surrounding bulk water^{12,14}. Further, plastisphere microbial communities could contribute to the acquisition and spread of pathogens and antibiotic resistance in aquatic environments¹⁵. These works suggest that the plastisphere is indeed capable of inducing negative effects at the ecosystem levels. However, the crucial roles of the plastisphere in biogeochemical cycling in marine environments are largely unknown.

Estuaries are the transitional areas between inland waters and remote oceans¹⁶, acting as hot zones for biogeochemical cycling. An estimated 1.2–2.5 million tons of plastic debris enter estuarine and coastal regions from inland rivers and lakes annually¹⁷. Therefore, any influence of plastics and the associated plastisphere on estuarine ecology and biogeochemical cycling could be particularly important. In addition to plastic contamination, estuaries are also subjected to unprecedented reactive nitrogen loads from anthropogenic activity, which leads to water eutrophication and ecological perturbations in estuaries^{18,19}. Under anoxic conditions, microbially mediated denitrification in estuarine waters, stepwise reductions of nitrate or nitrite to potent greenhouse gas N₂O or further to N₂²⁰, is the major process to eliminate the reactive nitrogen²¹. This pathway can alleviate the effects of eutrophication^{21,22}, but might contribute to global warming and ozone depletion²³. Therefore, attention on denitrification and associated N₂O productions should be paid in eutrophic estuarine regions. In the presence of plastic debris, microbial biomass in the plastisphere is likely considerable¹⁰, and anoxic microenvironments would occur during biofilm formation^{24,25}. Thus, the emerging plastisphere could harbor great but unrecognized potential in nitrogen removal and N₂O production. Elucidating the role of plastisphere in denitrification, especially in eutrophic waters, is of great significance for water quality remediation and climate change evaluation.

Research on denitrification processes in terrestrial and aquatic environments mainly focuses on bacterial denitrification (BD)^{22,26,27}. More evidence has shown that fungal denitrification (FD) and chemodenitrification (CD) could also contribute to nitrogen removal and formation of N₂O^{28–34}. Recent studies suggest that a high abundance of fungi, such as parasitic and saprophytic ones, could be attached to the plastic surfaces in aquatic environment³⁵. Moreover, fungal denitrifiers generally lack N₂O reductase, leading to N₂O as the end product^{36,37}. Thus, fungal denitrifiers may represent a potent contributor to N₂O production relative to bacterial denitrifiers (reduction of nitrate to N₂ as the end product). In addition, in organic matter- and iron-rich environments, iron (II) reacts with the reactive nitrogen to increase N₂O production from abiotic denitrification^{38–40}, which may also be a great contributor relative to BD. In fact, the importance of FD and CD in nitrogen transformation and N₂O production has been recognized across terrestrial ecosystems^{31,38,41}. However, their contributions in marine waters are largely unknown. Comparing to BD, whether FD and CD processes have similar importance for nitrogen removal and N₂O yield in marine plastisphere requires further investigation.

Here, we choose four types of plastics and establish in situ and lab-scale incubations in an estuary of Xiamen, China to investigate BD, FD, and CD potential in the plastisphere and to differentiate the contributions of these processes to N₂O production (experimental design, see Supplementary Fig. 1). We hypothesize that (i) the surface of plastic debris could be a site of plastisphere formation that provides the necessary conditions for denitrification, (ii) plastisphere has higher denitrifying activity than surrounding bulk water, and (iii) FD and CD processes may have a great contribution to N₂O production relative to BD. To test these hypotheses, we first measure messenger bis(3′–5′)-cyclic dimeric guanosine monophosphate (c-di-GMP), extracellular polymeric substances (EPS), and intracellular lipid/fatty acid levels to explore the plastisphere formation. Then the denitrifying activities in plastisphere and bulk water are detected by ¹⁵N isotope-pairing technique, and the relative contributions of BD, FD, and CD to total N₂O production are estimated using N₂O isotopocules analysis. Finally, the keystone bacterial and fungal denitrifiers of plastisphere and bulk water are identified. Our results fill a knowledge gap regarding biogeochemical cycling in the plastisphere and indicate that the new plastic niche may be a potential source of N₂O emission under global environmental change.

Results

Biofilm structure and activity. After the 30-d incubation in the estuary, the four types of plastic debris and surrounding bulk water were harvested. Using scanning electron microscope (SEM), we found that microorganisms in water were attached to the plastics and formed dense microbial clusters (Supplementary Fig. 2), suggesting biofilm formation on the surface of plastics.

We further explored anoxic microbial activities in the plastisphere and bulk water (Fig. 1). When cultured with heavy water (D₂O), assimilation of D by metabolically active cells into new biomass can be explicitly and quantitatively detected by Raman as a new C–D band (Fig. 1a). Thus the ratio of (C–D)/(C–D + C–H) is a quantitative indicator for microbial phenotypic activity^{15,42}. We acquired the Raman spectrograms of 40–50 microbial cells in each plastisphere and bulk water after 30 days, and calculated their (C–D)/(C–D + C–H) ratios. The ratios in each plastisphere (mean values 0.18–0.29) showed no statistical variations (Tukey, $P = 0.203–0.953$, Fig. 1b), but were greater than those in bulk water (mean value 0.09) ($P < 0.001$). This indicated a higher phenotypic activity in the plastisphere than in bulk water.

Biofilm composition, c-di-GMP, and lipid/fatty acid signals. A schematic diagram of microbial colonization processes on plastic surfaces in aquatic environments is illustrated in Fig. 2a. We detected the EPS contents (i.e., extracellular polysaccharide (PS), protein (PN), and DNA (eDNA)) in both the plastisphere and bulk water. As expected, the concentrations of PS, PN, and eDNA were all significantly greater than those in bulk water ($P < 0.001$, Fig. 2b–d). Except for PN and eDNA in the PVC plastisphere, no significant difference ($P = 0.125–0.669$) was detected among each plastic debris (Fig. 2b–d).

The intracellular second messenger c-di-GMP is associated with biofilm formation⁴³. We observed higher concentrations of c-di-GMP in the plastisphere (0.013–0.019 μg mg^{−1} protein) than in bulk water (below detection limit) ($P < 0.001$, Supplementary Fig. 3). This showed that high levels of c-di-GMP commonly support microbial growth in a sessile mode, whereas the low level could result in the planktonic mode²⁵. There were no obvious differences among the plastisphere formed by different plastic types ($P = 0.135–0.987$, Supplementary Fig. 3), suggesting that plastic types could not influence microbial c-di-GMP levels.

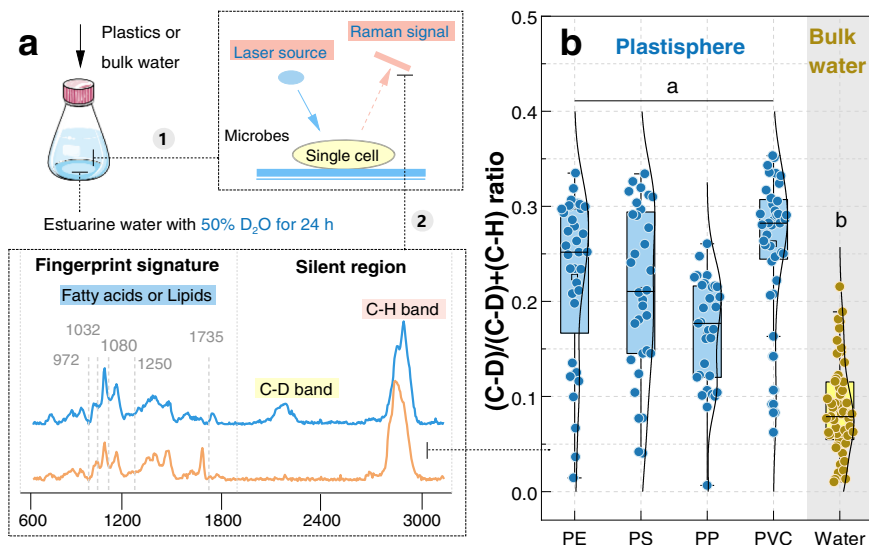


Fig. 1 D₂O-labeled single-cell Raman spectroscopy showing microbial metabolic activities under anoxic conditions in the plastisphere and bulk water. **a** Schematic diagram of the D₂O-labeled single-cell Raman technique. 1 represents the incubation and preparation of microorganism liquids; 2 represents Raman spectroscopy. Raman characteristic bands assigned to intracellular lipid/fatty acid biomolecules are pinpointed. **b** The ratios of (C-D)/(C-D)+(C-H) calculated from 40 to 50 single cells in the plastisphere and bulk water. Each point is a single cell. Different letters (a and b) indicate the significant differences ($P < 0.05$) among each plastisphere group and bulk water group.

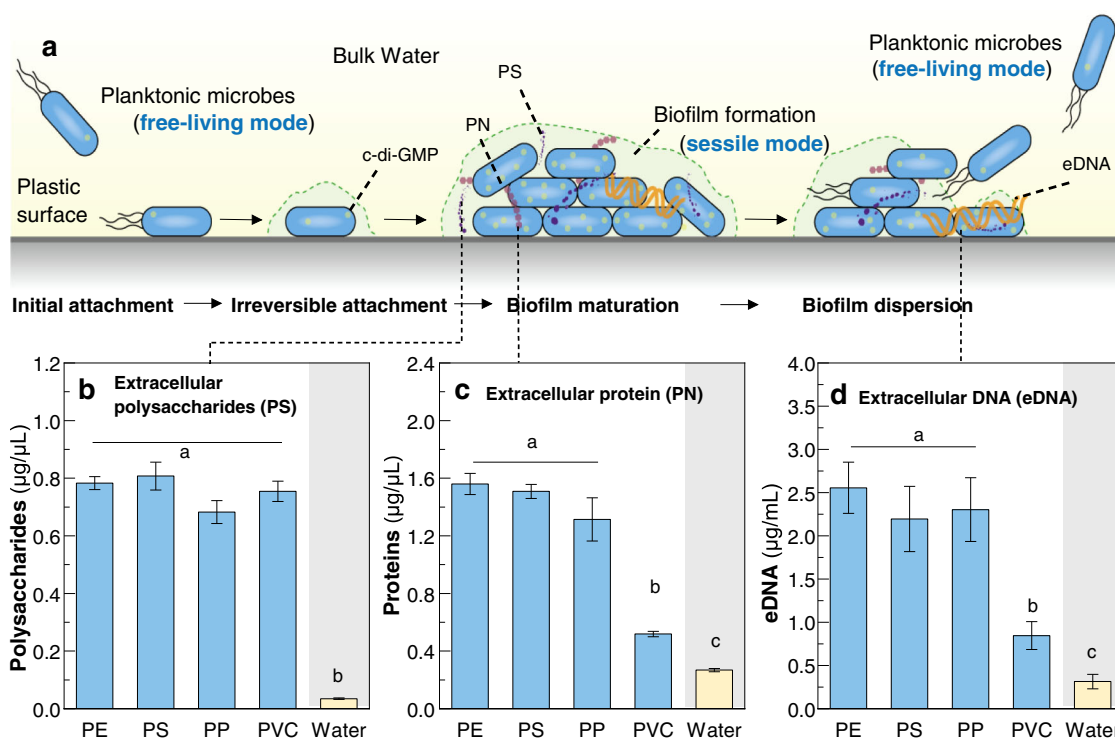


Fig. 2 Concentrations of extracellular polymeric substances (EPS) in the plastisphere and bulk water. **a** Schematic overview of biofilm formation and dispersion on plastic surfaces in water, including cell initial attachment, irreversible attachment, maturity, and dispersion. This diagram is modified from previous studies^{25,48}. **b-d** Concentrations of extracellular polysaccharide (PS), extracellular protein (PN), and extracellular DNA (eDNA). Error bars are the standard error. Different letters (a, b, and c) indicate the significant differences ($P < 0.05$) among each plastisphere group and bulk water group.

Microbial lipid and fatty acid levels may also be involved in biofilm formation and dispersion⁴⁴. Using D₂O-labeled single-cell Raman spectroscopy, a total of five characteristic bands assigned to lipid or fatty acids (i.e., 972, 1032, 1080, 1250, and 1735 cm⁻¹) were identified (Fig. 3). Among the five bands, the plastisphere had no striking difference in peak intensities with bulk water at the bands of 972 and 1735 cm⁻¹ ($P = 0.268-0.883$, Fig. 3a, e). At

1032, 1080, and 1250 cm⁻¹, however, the peak intensities in the plastisphere were lower than those in bulk water ($P < 0.001$, Fig. 3b-d), highlighting the different lipid/fatty acid levels in microorganisms between the plastisphere and bulk water.

Denitrification and N₂O production pathway. During the in situ incubation, the plastic debris was suspended in the water

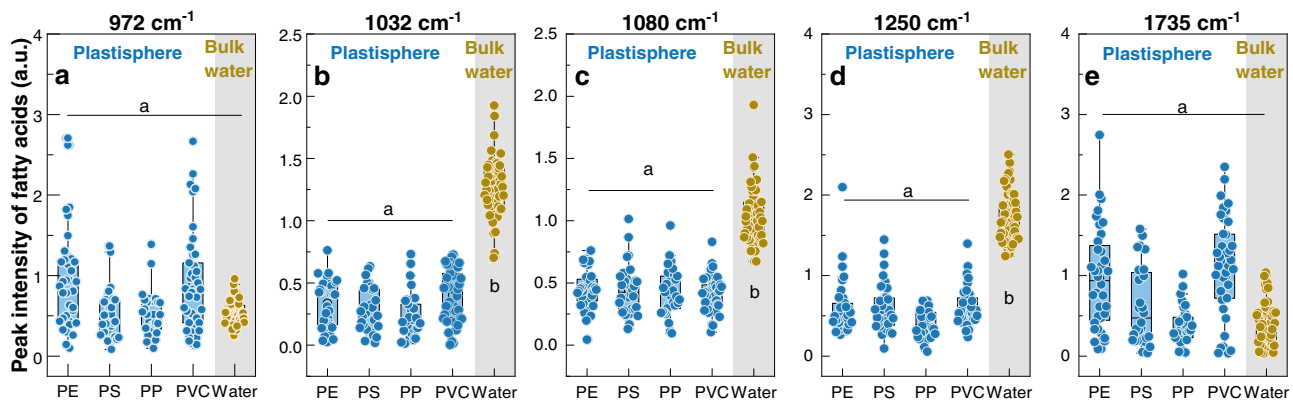


Fig. 3 Raman profiling of intracellular lipid/fatty acid levels in microorganisms of the plastisphere and bulk water. **a** 972 cm^{-1} . **b** 1032 cm^{-1} . **c** 1080 cm^{-1} . **d** 1250 cm^{-1} . **e** 1735 cm^{-1} . Different letters (a and b) indicate the significant differences ($P < 0.05$) among each plastisphere group and bulk water group.

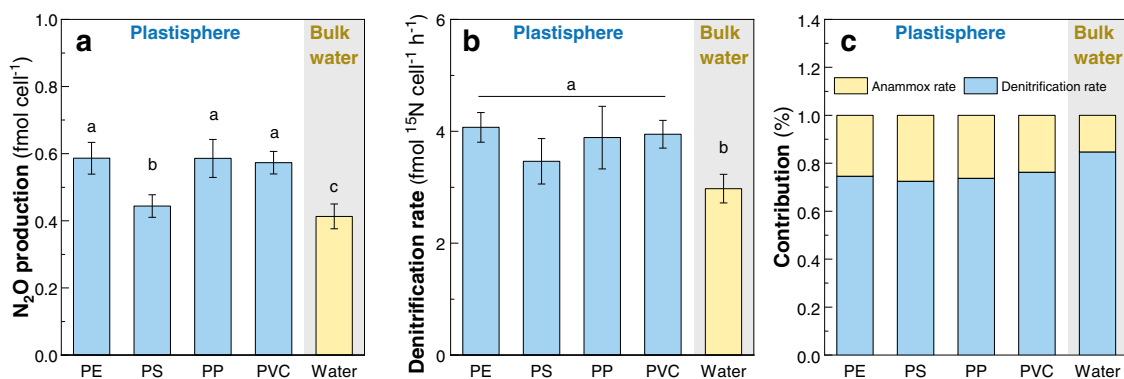


Fig. 4 Denitrifying activity and N_2O production in the plastisphere and bulk water. **a** Concentrations of N_2O after the 24 h denitrification experiment. **b** Denitrification rates quantified by ^{15}N isotope-pairing technique. Both N_2O production and denitrification rate are normalized with microbial cell numbers by using the absolute abundances of 16S rRNA in the plastisphere and bulk water (see “Methods”). **c** Contributions of denitrification and Anammox processes to N_2 production. Error bars are the standard error. Different letters (a, b, and c) indicate the significant differences ($P < 0.05$) among each plastisphere group and bulk water group.

depth of ~4 m, where the dissolved oxygen (DO) concentration was 1.19 mg L^{-1} ($< 2 \text{ mg L}^{-1}$, generally considered as hypoxia⁴⁵). Thus, we focused on the denitrification-derived N_2O in the lab-scale experiments of this study. Plastisphere and bulk water showed pronounced differences in denitrification rate and N_2O production (Fig. 4). After 24 h, N_2O concentrations were $0.44\text{--}0.59 \text{ fmol cell}^{-1}$ in the plastisphere, greater than $0.41 \text{ fmol cell}^{-1}$ in bulk water ($P < 0.001\text{--}0.042$, Fig. 4a). N_2O concentrations in the PS plastisphere were lower than the other types of plastisphere ($P < 0.001\text{--}0.012$). For denitrification rate, the plastisphere registered higher rates ranging from 3.36 to $4.07 \text{ fmol cell}^{-1} \text{ h}^{-1}$, while the bulk water had a lower rate (mean value $2.97 \text{ fmol cell}^{-1} \text{ h}^{-1}$) ($P = 0.001$, Fig. 4b). These corroborated that the plastisphere could be a potential source of denitrification and N_2O production. Comparing with Anammox process, denitrification contributed 73–84% of total N_2 productions (Fig. 4c), meaning the dominant role of denitrification in nitrogen removal in the estuary.

We further measured N_2O isotope values in the plastisphere and bulk water (Supplementary Fig. 4). Coupling $\text{N}_2\text{O}\text{-}\delta^{18}\text{O}$ with $\text{N}_2\text{O}\text{-SP}$ (site preference, see “Methods”) values, we could investigate the N_2O dynamics during denitrification. In the plastisphere, $\text{N}_2\text{O}\text{-}\delta^{18}\text{O}$ were $64.14\text{--}77.82\text{‰}$ and $\text{N}_2\text{O}\text{-SP}$ were $15.56\text{--}26.21\text{‰}$, while they were $55.62\text{--}59.93\text{‰}$ and $7.53\text{--}8.68\text{‰}$ in bulk water, respectively ($P < 0.001$, Supplementary Fig. 4), signifying a shift in N_2O production pathways. After calibration for oxygen exchange, a multiple-isotope plot ($\text{N}_2\text{O}/\text{H}_2\text{O}\text{-}\delta^{18}\text{O}$ vs

$\text{N}_2\text{O}\text{-SP}$) was generated (Fig. 5a). Considering N_2O mixing and reduction, we established a N_2O isotope-based mass balance model to differentiate the relative fractions of BD, FD, and CD processes to N_2O productions (see “Methods”). We found that BD was the major N_2O source, contributing $51.08\text{--}67.06\%$ and $77.10\text{--}79.59\%$ of total N_2O production in the plastisphere and bulk water, respectively ($P = 0.008$, Fig. 5b). FD unexpectedly contributed $8.55\text{--}46.40\%$ of total N_2O production, and the contribution in the plastisphere was higher than that in bulk water ($P < 0.001$, Fig. 5b). These demonstrated that the plastisphere exhibited a different N_2O production pattern from bulk water. Comparing with BD and FD, the proportion of the CD process ($0\text{--}10.28\%$) can be ignored, for both plastisphere and bulk water.

Denitrifier communities. We first quantified the abundances of 16S rRNA and ITS genes in the plastisphere and bulk water (Supplementary Fig. 5), and found that the abundances of bacteria and fungi were higher in the plastisphere than those in bulk water ($P < 0.001\text{--}0.027$). Denitrifier communities were then investigated by high-throughput sequencing based on three denitrifying marker genes (i.e., bacterial *nirS* (*bnirS*), bacterial *nirK* (*bnirK*), fungal *nirK* (*fnirK*)). As indicated by α -diversity, the plastisphere had a higher diversity and richness than bulk water ($P < 0.05$, Supplementary Fig. 6). The diversity of *bnirS*-type denitrifiers reached the highest, followed by *fnirK*-type and

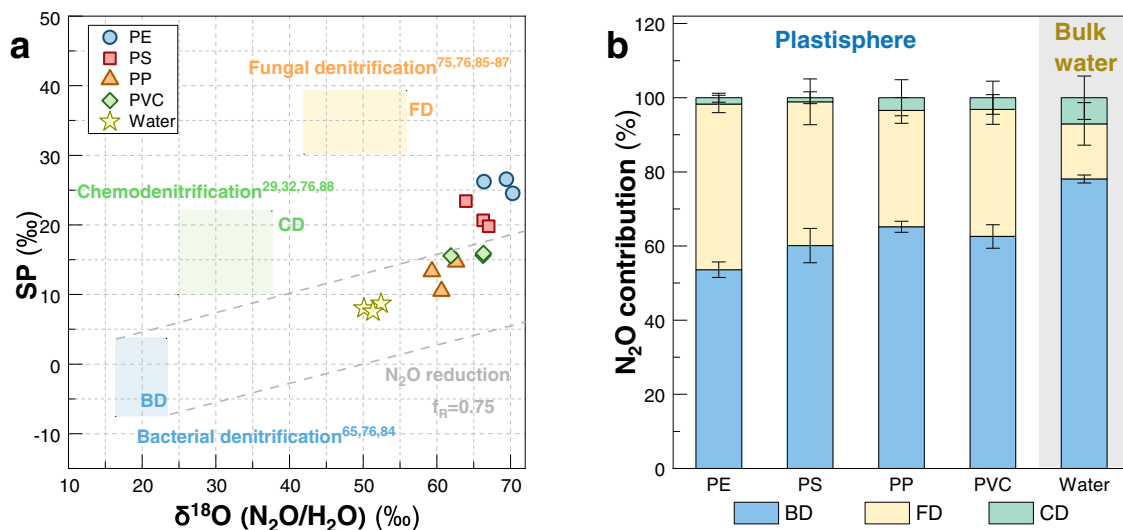


Fig. 5 Multiple-isotope signatures of N₂O illustrating the relative contributions of bacterial denitrification (BD), fungal denitrification (FD), and chemodenitrification (CD) in the plasticsphere and bulk water. **a** Relationships between N₂O-SP and N₂O-δ¹⁸O (N₂O/H₂O) values in each group.

N₂O-δ¹⁸O values were corrected for H₂O-δ¹⁸O assuming almost complete O exchange. Ranges of putative isotope signatures of N₂O (δ¹⁸O (N₂O/H₂O)) from BD, FD, and CD are indicated as the three color boxes. The corresponding references are listed in the figure. The area enveloped by gray dash lines represents the N₂O reduction through BD process based on fractionation effects (slope = SP_{eN₂O}/δ¹⁸O_{eN₂O} = 0.25). This mapping approach is modified from the method in ref. ⁸³ **b** Relative proportions of N₂O production via BD, FD, and CD in the plasticsphere and bulk water. Errors were estimated by Monte Carlo simulation and reflected the accuracy of N₂O isotope mass balance model. Although the contributions of each denitrification process would shift with the prescribed extent of oxygen change and N₂O-SP and N₂O-δ¹⁸O values, all ranges suggest that biotic denitrification instead of chemodenitrification was the main contributor to N₂O production in the plasticsphere and bulk water.

by *bnirK*-type denitrifiers. In light of the Bray-Curtis distances (Fig. 6a), the three denitrifier communities between plasticsphere and bulk water clearly formed two separated clusters ($P < 0.01$, $R = 0.873-0.927$). No obvious or separated clusters among the four plastic debris were observed. As shown in Supplementary Fig. 7, the major phylum was Proteobacteria in *bnirS*-type and *bnirK*-type denitrifier communities, and it was Ascomycota and Basidiomycota in *fnirK*-type denitrifier communities. However, their relative abundances varied greatly between plasticsphere and bulk water, implying a distinct denitrifier structure between these compartments. We also found that plastic types did not obviously change the denitrifier compositions and relative abundances (Supplementary Fig. 7), albeit with some variations in *bnirK*-type denitrifier community at the genus level for the polystyrene (PS) type.

Co-occurrence network analysis showed that the plasticsphere harbored more complex interactions among the three denitrifier communities in comparison with bulk water (Fig. 6b and Supplementary Table 1). We found that the keystone genera of denitrifiers were shifted between plasticsphere and bulk water. In the plasticsphere, the *bnirK*-type denitrifiers (*Pseudomonas*, *Bosea*, *Ochrobactrum*, and *Starkeya*) accounted for the main keystone genera, while *bnirS*-type denitrifiers (α,β -Proteobacteria and *Azoarcus*) were dominant in bulk water (Fig. 6b). *fnirK*-type keystone denitrifiers were also changed from *Talaromyces*, *Chaetomium*, and *Penicillium* in the plasticsphere to *Fusarium*, *Alternaria* and *Trichosporon* in bulk water. Such shifts probably explained the different denitrifying activities between plasticsphere and bulk water. In addition, we also quantified the relative abundances of *narG*, *nirS*, *nirK*, and *nosZ* (Supplementary Fig. 8). Plasticsphere generally contained higher abundances than the bulk water ($P = 0.001-0.038$), partially explaining the higher denitrification rates in the plasticsphere.

We further explored the denitrifier-based niche breadth and overlap at community level. Niche breadths of all three denitrifier communities in the plasticsphere were greater than those of bulk

water ($P < 0.001$, Fig. 6c). This indicates that plastic surfaces could offer more opportunities for denitrifiers attachment and biofilm development than the surrounding water⁴⁶. In line with the results of niche breadth, the plasticsphere also presented a higher niche overlap level ($P < 0.001$, Fig. 6d), which reflects a sharp competition in denitrifier communities for energy and nutrients in comparison with bulk water⁴⁷.

Discussion

The potential of plasticsphere in global nitrogen cycling and associated greenhouse gas flux is rarely examined. Our study provides evidence of the plasticsphere exhibiting a higher denitrifying activity compared to bulk water and functioning as a neglected source of greenhouse gas N₂O production. Below, we discuss the likely reasons for these findings.

In our study, higher levels of PS, PN, and eDNA were observed in the plasticsphere comparing with bulk water (Fig. 2b-d). This indicates that the estuarine microbes secrete EPS and then grow within the self-produced extracellular matrix to form biofilms during their colonization on plastic debris^{24,48}. We also found that the EPS concentrations were coordinated with the c-di-GMP levels that were higher in the plasticsphere and lower in bulk water (Supplementary Fig. 3). This is likely because microbial secretion of EPS and biofilm formation are mainly regulated by the intracellular c-di-GMP level, especially in the Proteobacteria phylum^{25,43}. Recent studies have demonstrated that higher c-di-GMP levels could enhance EPS yields through repressing the expression of transcription factor FleQ (*P. aeruginosa*)⁴⁹ or increasing the surface adherence and immobility organelles such as T4P (*V. cholerae* and *C. difficile*)⁵⁰. In addition, c-di-GMP is also capable of downregulating flagellar expression (*P. aeruginosa*), reducing flagellar assemblies (*C. crescentus*)⁴³, or perturbing flagellar motor function (*E. coli*)⁵¹, which suppresses the motility and gradually forms biofilms. Therefore, the elevated c-di-GMP levels in the plasticsphere are important for EPS production and biofilm formation on the plastic debris.

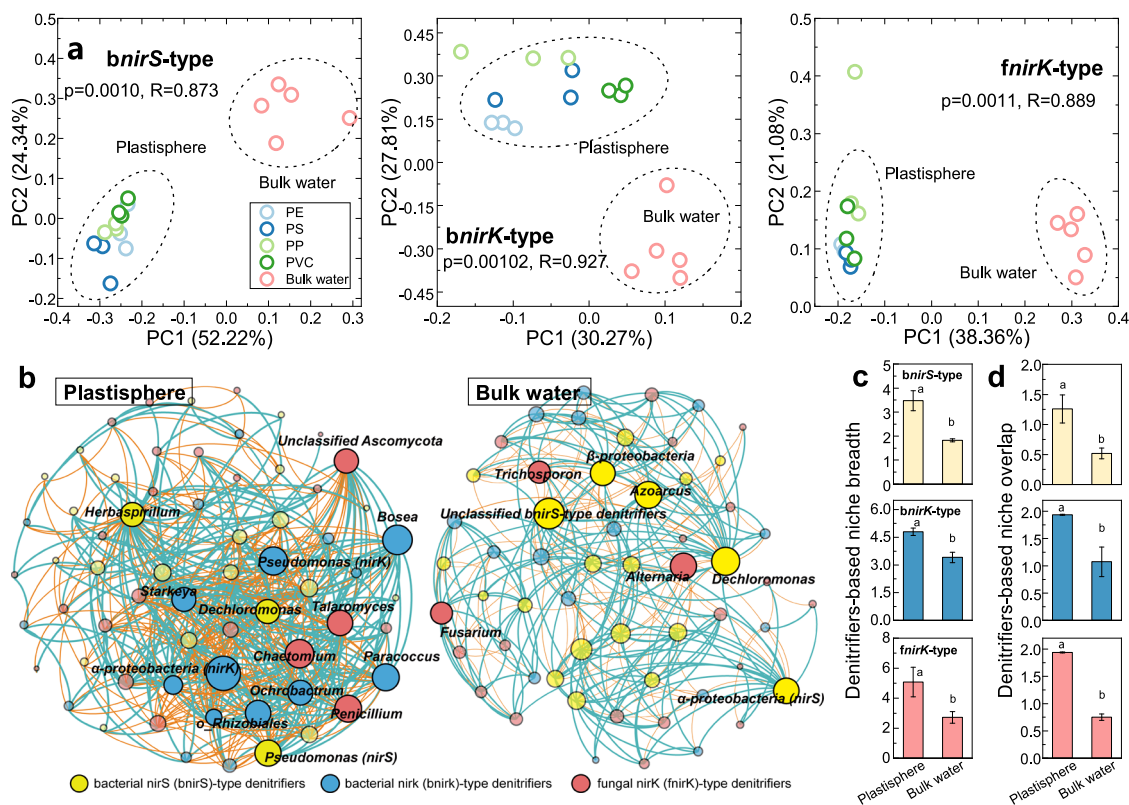


Fig. 6 Denitrifier community in the plastisphere and bulk water. **a** Principal coordinates analysis with ANOSIM test showing the differences in community structures of *bnirS*-type, *bnirK*-type, and *fnirK*-type denitrifiers between plastisphere and bulk water. **b** Co-occurrence network analysis illustrating the keystone denitrifiers (nodes, $R^2 > 0.9$, $P < 0.05$) in the plastisphere and bulk water. The parameters of the networks are listed in Supplementary Table 1. *bnirK*-type denitrifiers dominated in the keystone taxa in the plastisphere, while *bnirS*-type ones were the main keystone in bulk water. **c, d** Niche breadth and overlap based on the three types of denitrifier communities. Error bars are the standard error. Different letters (a and b) indicate the significant differences ($P < 0.05$) between plastisphere and bulk water.

Another important finding is that microbial lipid and fatty acid levels were lower in the plastisphere than in bulk water (Fig. 3). Intracellular lipid/fatty acid signals are reported to be involved in biofilm formation and dispersion⁴⁴. Accumulations of lipid/fatty acids in microorganisms could activate the activity of phosphodiesterases (catalyzing *c*-di-GMP consumption pathway), leading to lower *c*-di-GMP levels and biofilm dispersion²⁵. Moreover, lipid/fatty acid signaling molecules, such as *cis*-2-decenoic acid, *cis*-11-methyl-2-dodecenoic acid, and *cis*-2-dodecenoic acid, are capable of dismantling small microaggregates and inhibiting biofilm formation^{52,53}. For example, previous studies have shown that biofilm roughness, thickness, and biomass were significantly reduced in the presence of *cis*-2-decenoic acid⁵². This is likely because these signaling molecules could maintain bacterial and fungal cells metabolically active, benefit for dispersive growth. Thus, the lower intracellular lipid/fatty acid levels observed here might be another important reason for the biofilm formation on the plastics.

During biofilm formation, surfaces of plastics are more likely to recruit anoxic denitrifiers, which is substantiated by the higher abundances of denitrifiers and denitrifying genes in the plastisphere than in bulk water (Supplementary Figs. 7 and 8). Low concentrations of dissolved oxygen in biofilms may account for the result. In biofilms, a steep gradient of dissolved oxygen could occur from outer to inner spaces, and thus produce anoxic conditions^{54,55}. Since denitrifiers can utilize nitrate/nitrite as electron acceptors instead of O_2 to support their metabolisms²⁰, the oxygen-limited conditions are favorable for their growth and activity. The higher anoxic activities in the plastisphere (Fig. 1)

further supported this explanation. In addition, we also found that the bacterial denitrifiers in the plastisphere mainly belonged to Proteobacteria phylum (Supplementary Fig. 7), consistently with previous studies indicating that Proteobacteria was the globally most abundant on surfaces of marine plastics⁵⁶. Many members of Proteobacteria (such as *Pseudomonas*) display strong capacities of EPS secretion and have evolved a “holdfast”⁵⁷. Thus, these denitrifiers may be favored compared to other microorganisms for surface attachment onto plastic debris. Taken together, our study revealed that, on contact with the plastic debris, estuarine microorganisms produced EPS to form biofilm by the regulation of *c*-di-GMP and lipid/fatty acid signals. The subsequently generated anoxic microsites could provide opportunities for denitrifiers, and thereby resulted in the higher denitrifying activity in the plastisphere, supporting our first hypothesis.

Denitrification and N_2O production were recorded in the plastisphere and bulk water (Fig. 4). The observed denitrification rates are of comparable magnitude to previous studies conducted in remote oceans⁵⁸, coastal, and estuarine sediments²¹, suggesting the importance of the denitrification process in marine ecosystems. Comparing with bulk water, plastisphere had greater denitrification rates and N_2O productions (Fig. 4), which supports our second hypothesis. It can be soundly attributed to the differences of denitrifier communities and biomasses between plastisphere and bulk water. Our study showed that the niche breadths of denitrifier communities in the plastisphere were higher than that of bulk water (Fig. 6c), implying that more denitrifiers are likely to be attached to the plastics than to freely

live in water^{14,46}. Network analysis further indicated that *bnirK*-type denitrifiers dominated in the keystone taxa of plastisphere, whereas *bnirS*-type ones were the core residents in bulk water (Fig. 6b). In comparison with *bnirS*-type denitrifiers, *bnirK*-type ones could display strong adaptability to fluctuating environments (i.e., dissolved oxygen)⁵⁹, and thus are more easily attached onto the plastics. Furthermore, *bnirK*-type denitrifiers are more effective for nitrite reduction and N₂O production than *bnirS*-type ones⁶⁰. This is further evidenced by the greater ratios of (*nirS* + *nirK*)/*nosZ* (1.5–2.3) in the plastisphere than those (0.33–0.41) in bulk water (Supplementary Fig. 8). All of these accounted for the stronger denitrifying capability in the plastisphere.

Using the mass balance model, we found that BD dominated in N₂O production in both the plastisphere and bulk water (Fig. 5b). Generally, the oxygen-limited conditions are more favorable for BD process. The bacterial denitrifiers (*bnirS*- or *bnirK*-type), identified as the main keystone taxa in the plastisphere and bulk water (Fig. 6b), further supported the bacterial dominance in N₂O productions. The bacterial proportions in this study (51–79%) were higher than those of previous studies conducted in coastal (14–60%)²⁸ and estuarine (15–21%)⁶¹ sediments, suggesting a spatial heterogeneity of BD in marine ecosystems. In addition, we noticed that the bacterial contributions to N₂O production had no striking difference among the four types of plastics (Fig. 5b), which signifies the intrinsic importance of BD, rather than an opportunistic response in the estuarine plastisphere. The enhanced contribution of BD is favorable for reactive nitrogen removal by the transformation to N₂O and N₂. This implies that BD is an important source for greenhouse gas N₂O.

Fungal contributions to N₂O production in estuarine water have been less well studied. It generally derives from two pathways including FD and fungi-mediated codenitrification³¹. During codenitrification with the addition of ¹⁵N-nitrate/nitrite, fungi would form more hybrid ⁴⁵N₂O and ²⁹N₂ than ⁴⁶N₂O and ³⁰N₂^{62,63}. In our ¹⁵N-labeling experiment, however, we detected a large portion of ³⁰N₂ rather than ²⁹N₂, indicating that the codenitrification contribution to N₂O production was less in this study. Fungal N₂O production could thus be mainly from FD process. Our study further showed that the contributions of FD to total N₂O productions were 8–46% in the plastisphere and bulk water (Fig. 5b). This highlighted the non-negligible role of fungal denitrifiers in N₂O production, despite the proportions being lower than those in marine sediments (40–70%)²⁸, which partially supports our third hypothesis. Moreover, we found higher proportions of N₂O production from FD in the plastisphere (26–46%) than in bulk water (8–22%, Fig. 5b). Fungal niche selection may account for the different N₂O production patterns between plastisphere and bulk water, because the aquatic microorganisms are prone to nesting in more fragmented habitats like plastic debris rather than in water¹⁴. The biofilms formed by attached microbes promote cellular interactions, thus likely leading to the distinct N₂O dynamics between plastisphere and bulk water.

The small contribution of CD to N₂O production (0–10.28%) indicated that CD is not an important N₂O contributor in both the plastisphere and bulk water (Fig. 5b). By contrast, Wankel et al.²⁸ and Wang et al.³⁸ documented that the contributions of CD to N₂O production could reach 31–75% in paddy soils and coastal sediments. The different results were probably caused by the different iron contents that play an essential role in the CD process⁶⁴. In soils and sediments, the chemical reactions of particle-bound reduced iron with various enzymatically-derived electron acceptors (i.e., hydroxylamine, nitric oxide or nitrite) can contribute to pronounced yields of N₂O⁶⁴. In our study, however, the iron concentrations were low (2.89–7.95 mg L⁻¹), thus likely limiting the importance of the CD process in estuarine water.

It is worth noting that the nitrification process in the plastisphere and bulk water, including hydroxylamine oxidation and nitrifier denitrification^{41,65}, may also contribute to N₂O production. We further conducted a lab-scale experiment under in situ dissolved oxygen concentration (~1.2 mg L⁻¹, hypoxic conditions) to explore nitrifier potential in N₂O production in the plastisphere and bulk water (Supplementary Fig. 9). There was no significant difference observed between groups with and without adding allylthiourea (a nitrification inhibitor⁶⁶), indicating that N₂O production via hydroxylamine oxidation was minimal under in situ conditions. By contrast, nitrifier denitrification was likely a potential contributor in the plastisphere and bulk water (Supplementary Fig. 9b), but the concentration was lower than that of denitrification-based N₂O. More importantly, the nitrifier denitrification-based N₂O production in the plastisphere was higher than in bulk water (Supplementary Fig. 9). This further supports that the plastisphere is an overlooked source of N₂O production. Although in-depth discussions on the nitrifier-related sources of N₂O are beyond the scope of this study, we believe that it is urgent to investigate nitrification and associated N₂O dynamics in future research, which will deepen the understanding of the role of aquatic plastisphere in biogeochemical cycling.

Plastisphere derived from the widespread dissemination of plastic debris in estuarine environments⁸, is changing the stability and function of the ecosystem^{12,14}. Our results reveal that the plastisphere produces approximately twofold greater emissions of the potent greenhouse gas N₂O from denitrification pathways than the bulk water. By further assessing Global Warming Potential (GWP) of N₂O production⁶⁷, we also find that plastisphere exhibits the higher warming potential (34.86–41.12 mg CO₂ eq L⁻¹ d⁻¹) than the bulk water (13.15–17.26 mg CO₂ eq L⁻¹ d⁻¹). Both of these indicate that the emerging plastisphere could be a great but neglected source of anthropogenic N₂O. Although our data could not make precise estimations of N₂O flux and its warming potential from global plastisphere, the importance of estuarine plastisphere in N₂O production via anthropogenic sources should be recognized, especially under global climate change. It is estimated that annual emissions of plastic debris to marine ecosystems are 5–13 million tons⁸, and the biomass on these plastics could be 0.2–6% of total microbial biomass in marine surface waters¹⁰. Given the substantial plastic waste and microbial biomass, future research at larger scales is needed to make reliable predictions of N₂O fluxes from plastisphere and to evaluate the warming potential of N₂O production from pervasive plastisphere across global marine ecosystems.

Methods

Study site, plastic preparation, and experimental design. In this study, the in situ incubations were conducted in an estuary of Xiamen, China (118°07'E, 24°61'N–118°09'E, 24°59'N) during April and May 2021. This region possesses a subtropical maritime monsoon climate, and has an average temperature of 21 °C and receives 1100 mm of rain⁶⁸. Owing to human activities, pollutants in rainwater runoff and a portion of wastewater have been recently transported to the estuary, leading to reduced water quality and slight eutrophication. We sampled the estuarine water at 4 m depth and determined its characteristics. The water (pH 6.5, 20 °C) contained 1.19 mg L⁻¹ dissolved oxygen, 21.2–25.7 mg L⁻¹ total organic carbon, 0.72–0.99 mg L⁻¹ nitrate, 0.19–0.43 mg L⁻¹ ammonium, 0.09–0.17 mg L⁻¹ nitrite, and 2.89–7.95 mg L⁻¹ iron.

Four types of common commercial plastics, i.e., polyethylene (PE), polystyrene (PS), polypropylene (PP), and polyvinylchloride (PVC), were selected. They have a low bioreactivity with densities of 0.88–0.97 g cm⁻³. The PE-type food bags were from Cleanwrap Co., China. PS was obtained from transparent plastic cups (Chuanguan Co., China). PP was from sealable plastic bags from Xingmin Co., China. The PVC-type cling films were donated by Jusu Co., China. The four types of plastics were cut into a size of ~10 × 10 cm for subsequent experiments.

To investigate the denitrifying capability of the plastisphere, we performed (1) an in situ incubation for 30 days (30d), and (2) a subsequent denitrification experiment for 24 h (24h). The detailed experimental design is illustrated in Supplementary Fig. 1. At the initial stage of in situ incubation, the obtained 10 × 10-cm plastic debris was sterilized using 70% ethanol and connected with

cotton cords, and we used stone debris placed under the plastics to maintain buoyancy. This led to a ~4 m water depth for the plastics suspended in estuarine water. After 30 days, the plastic debris and surrounding bulk water (10 L) were harvested with a polymethyl-methacrylate sampler (Haifuda, China). A portion of plastics and bulk water was used for water quality analysis, SEM, and D₂O-labeled single-cell Raman spectroscopy. The remaining material was used for the preparation of plastisphere suspensions and the subsequent 24 h experiment. Methods for water quality detections and SEM are listed in Supplementary Methods 1 and 2.

Prior to the denitrification experiment, a portion of bulk water was first filtered through a 0.22- μ m polycarbonate membrane to remove microorganisms and then transferred into 250-mL sterile beakers. Thereafter, the collected plastic debris was placed in these beakers, and biofilms were repeatedly shaken, agitated, and washed with the sterile bulk water until a large proportion of the biofilms were detached⁶⁹. Plastisphere suspensions were then collected for the determinations of denitrification rate, N₂O reduction ratio (f_R), EPS and c-di-GMP levels, and further experiments (Supplementary Fig. 1). During the 24 h denitrification experiment, we established plastisphere groups (i.e., plastisphere suspensions of PE, PS, PP, and PVC) and a bulk water group (estuarine water). Each plastisphere group was presented in triplicate, and the bulk water group (in quintuplicate) was set as control. Forty milliliters of plastisphere suspensions and bulk water were transferred into 120-mL serum bottles, respectively. Next, these bottles were sealed, purged with high-purity He (>99.99%) for 5 min, and incubated at 20 °C for 24 h. No additional carbon or nitrogen source was added, aiming to explore the basal capacities of denitrification in the plastisphere and bulk water. Each lab-scale experiment was conducted in parallel, and variations in the concentrations of organic matter during the lab-scale experiment are shown in Supplementary Fig. 10. After 24 h, N₂O concentration and isotopocules, denitrifier community, and gene abundance in the plastisphere and bulk water were measured.

In this study, we prepared the plastisphere suspensions, aiming to explore the biofilms on the plastics under more controlled conditions during the lab-scale experiments. To examine if the growth pattern (attached or detached biofilms) has significant impacts on microorganisms during the 24 h experiment, we further investigated N₂O production, anoxic microbial activities, and community structure of the attached and detached biofilms (Supplementary Fig. 11). These results showed no significant differences between attached and detached biofilms, suggesting that denitrifier activities during 24 h were not likely to be significantly impacted by growth patterns. In addition, we selected the water volume of 40 mL to conduct the 24 h experiment, because it is the minimum volume for a large proportion of biofilm detachment from plastic debris. We also conducted the same experiments with different volumes (80 and 120 mL) to avoid bias induced by incubation water volume (Supplementary Fig. 12). The results showed that N₂O production in the plastisphere was higher than that in bulk water, regardless of water volumes.

In addition, it should be noted that marine particle debris is mainly in the form of plastics, occupying up to 60–80%⁷⁰. Moreover, other particle fragments such as glass, metal, or stone, could be deposited to marine sediments, and the direct effects of these particles on marine waters are minor. Therefore, we only consider the plastic debris in this study.

EPS and c-di-GMP detections. After the 30-d incubation, the EPS and c-di-GMP concentrations in the plastisphere and bulk water were measured. Extractions of EPS were following the formaldehyde-NaOH method⁷¹. Plastisphere suspension (3 mL) or bulk water (3 mL) together with 2 mL sterile phosphate buffer were transferred into a 15-mL centrifuge tube. After centrifugation (5000 \times g, 4 °C, 5 min) and removal of the supernatant, 5 mL of sterile phosphate buffer and 50 μ L of 37% formaldehyde were added to re-suspend the pellet. The tube was shaken for 5 min and stored at 4 °C for 60 min, and then 2 mL of 1 M NaOH was added. After being stored at 4 °C for 3 h, the supernatant was harvested by centrifugation (5000 \times g, 4 °C, 10 min) and used for PS, PN, and eDNA detections after filtering through a 0.22- μ m polycarbonate membrane. PS concentration was measured at $\lambda = 625$ nm following the Anthrone method using glucose as standard. PN concentration was determined at $\lambda = 562$ nm by a Protein Assay Kit (Beyotime Biotechnology, China) using BSA as standard. eDNA concentration was quantified at $\lambda = 260$ nm by a DNA Detection Kit (QuantiFluor, dsDNA system, USA).

Microbial c-di-GMP in the plastisphere and bulk water were extracted and measured based on previous studies^{72,73}. The extraction solvent consisted of acetonitrile/methanol (50/50, v/v). Cells in the plastisphere suspension and bulk water were disrupted using ultra-sonication for 5 min (120 W, 4 °C), and then transferred into a 15 mL centrifuge tube. After adding 8 mL extraction solvent and vortexing for 60 s, the suspensions were maintained at –80 °C for 2 h, and the supernatants were collected by centrifugation (14,000 \times g, 15 min). Thereafter, a pressured gas blowing concentrator (HGC-12A, Hengao, China) was used to dry the supernatants under continuous flows of N₂. The residues were resuspended in 500 μ L of ultrapure water for subsequent detection of c-di-GMP. The concentration of c-di-GMP was detected with an LC-MS/MS equipped with an electrospray ionization source (Applied Biosystems 6500, USA) at a reversed-phase. The $m/z + 689/150$ and $+ 689/343$ quantifiers were c-di-GMP transitions. Declustering potential (DP) was –185 and collision energy (CE) was –45 and –48. The obtained peak areas were compared with a calibration curve generated with a c-di-

GMP standard (Sigma-Aldrich, Germany). Concentrations of intracellular proteins were measured using a Protein Assay Kit (Beyotime Biotechnology, China).

Denitrification rate and N₂O isotope measurement. After the 30-d incubation, denitrification rates of the plastisphere and bulk water were measured using the ¹⁵N isotope-pairing technique^{21,74}. Five milliliters of plastisphere suspension or bulk water were prepared and transferred to a 12 mL gas-tight vial (Labco Exetainer, UK). The vials were purged with high-purity He (99.99%) for 5 min to replace the headspace air. The samples were first pre-incubated at 20 °C for 24 h to remove residual nitrate. After the removal, the vials were spiked with K¹⁵NO₃ solution (99.8% atom, Macklin Co. China) to reach a concentration of 200 μ M ¹⁵NO₃[–] on the basis of in situ concentrations, and then re-purged with high-purity He. The samples were incubated in dark for 8 h at 20 °C. After the incubation, 2 mL of headspace gas was taken by a syringe and transferred to a new 12 mL vial pre-filled with He gas. The concentrations of ²⁸N₂, ²⁹N₂, and ³⁰N₂ in the headspace were quantified with a GasBench-II/isotope ratio mass spectrometry (Thermal Delta V Advantage, Germany). The detection limit is 0.1 μ M. The denitrification rate was calculated as follows:

$$\text{Denitrification rate (mg}^{15}\text{ N L}^{-1}\text{ h}^{-1}) = \frac{T_{30} \times 2 \times (1 - F_n)}{F_n} + 2 \times T_{30} \quad (1)$$

where T_{30} (mg ³⁰N₂ L^{–1} h^{–1}) represents the production rates of ³⁰N₂ during the 8 h. F_n (99%) is the ¹⁵N fraction in added ¹⁵NO₃[–] to residual ¹⁵NO₃[–] after pre-incubation.

After the 24-h denitrification experiment, the headspace gas from the 120-mL serum bottle was taken to measure N₂O concentrations and isotopic compositions. Three milliliters of headspace gas was used to analyze N₂O concentration with a gas chromatograph (7890A, Agilent Technologies, USA), and 1 mL of headspace gas was used to detect N₂O isotope compositions, including $\delta^{15}\text{N}^{\text{bulk}}$, $\delta^{15}\text{N}^{\alpha}$, $\delta^{15}\text{N}^{\beta}$, and $\delta^{18}\text{O}$, with a Precon+Gasbench/isotope ratio mass spectrometer (Delta V plus, Thermal, USA)⁷⁵. Of these, ¹⁵N ^{α} (central, ¹⁴N–¹⁵N–¹⁶O) and ¹⁵N ^{β} (terminal, ¹⁵N–¹⁴N–¹⁶O) are the isotopocules⁷⁶. N₂O gas in samples was first enriched in liquid N₂ trap, purified, and then separated by a gas chromatography column (30-m long, 0.32-mm i.d.). Next, high-purity He flowing at 2 mL min^{–1} was applied to transport the N₂O gas to the mass spectrometer. N₂O isotopocules were detected by simultaneously capturing NO⁺ (m/z 30, 31) and N₂O⁺ (m/z 44, 45, 46). The scrambling factor was determined as 0.085. In this study, the isotopocule values of the internal reference gas (high-purity N₂O (>99.99%)) were pre-analyzed in Thünen Institute of Climate-Smart Agriculture, Germany. Two standard gases provided by Dr. Anette Goeske and Dr. Reinhard Well were applied to perform two-point calibrations for values of N₂O site preference (N₂O-SP, AKI N₂O-SP = –2‰, Mix 1 N₂O-SP = 15‰, 5ppm). Values of $\delta^{15}\text{N}^{\text{bulk}}$, $\delta^{15}\text{N}^{\alpha}$, $\delta^{15}\text{N}^{\beta}$, $\delta^{18}\text{O}$, and SP of N₂O were calculated as follow:^{77,78}

$$\text{N}_2\text{O} - \delta^{15}\text{N}^i(\text{‰}) = ({}^{15}\text{N}_{\text{sample}} - {}^{15}\text{N}_{\text{standard}}) / {}^{15}\text{N}_{\text{standard}} (i = \alpha \text{ or } \beta) \quad (2)$$

$$\text{N}_2\text{O} - \delta^{18}\text{O}(\text{‰}) = ({}^{18}\text{O}_{\text{sample}} - {}^{18}\text{O}_{\text{standard}}) / {}^{18}\text{O}_{\text{standard}} \quad (3)$$

$$\text{N}_2\text{O} - \delta^{15}\text{N}^{\text{bulk}}(\text{‰}) = (\delta^{15}\text{N}^{\alpha} + \delta^{15}\text{N}^{\beta}) / 2 \quad (4)$$

$$\text{N}_2\text{O} - \text{SP}(\text{‰}) = \delta^{15}\text{N}^{\alpha} - \delta^{15}\text{N}^{\beta} \quad (5)$$

where $\delta^{18}\text{O}$ and $\delta^{15}\text{N}^i$ are the ratios of ¹⁸O/¹⁶O and ¹⁵N/¹⁴N, respectively. $\delta^{15}\text{N}^{\alpha}$ and $\delta^{15}\text{N}^{\beta}$ denote the ratios of ¹⁴N–¹⁵N–¹⁶O and ¹⁵N–¹⁴N–¹⁶O, respectively. All values were presented as ‰ relative to atmospheric N₂ (¹⁵N) or Vienna Standard Mean Ocean Water (¹⁸O). The typical detection precisions are 0.3‰ (N₂O- $\delta^{15}\text{N}^{\text{bulk}}$), 0.9‰ (N₂O- $\delta^{15}\text{N}^{\alpha}$), 0.9‰ (N₂O- $\delta^{15}\text{N}^{\beta}$) and 0.6‰ (N₂O- $\delta^{18}\text{O}$).

Correction of N₂O- $\delta^{18}\text{O}$ and N₂O isotope mass balance model. During denitrification, the incorporation of the oxygen atom from H₂O into N₂O or nitrate could affect the measured $\delta^{18}\text{O}$ values of N₂O (N₂O- $\delta^{18}\text{O}$)^{75,79,80}. Previous studies conducted in soils suggest that an almost oxygen exchange occurred during denitrification⁷⁹. Therefore, assuming a complete O exchange $\delta^{18}\text{O}$ values of the ambient water (H₂O- $\delta^{18}\text{O}$) could be used for interpretation. As the variation of H₂O- $\delta^{18}\text{O}$ values in global surface seawater is minor⁸¹, we used a theoretical H₂O- $\delta^{18}\text{O}$ value (0.91‰, between –2.98 and 1‰)^{81,82} reported in the literature for seawater to correct the measured N₂O- $\delta^{18}\text{O}$ values (subtracting H₂O- $\delta^{18}\text{O}$ value).

After correction, the multiple-isotope relationships between N₂O-SP and N₂O- $\delta^{18}\text{O}$ were plotted based on the mapping approach⁸³, which was first applied by Lewicka-Szczepak et al. Then, we further established a N₂O isotope mass balance²⁸ to explore the relative fractions of N₂O-producing sources in the plastisphere and bulk water. As the denitrification experiment was anaerobically executed, N₂O productions via BD, FD, and CD processes were taken into account. Fractions of BD (f_{BD}), FD (f_{FD}), and CD (f_{CD}) pathways to total N₂O flux were expressed as follow:

$$\text{Total N}_2\text{O production} = f_{\text{BD}} + f_{\text{FD}} + f_{\text{CD}} = 1 \quad (6)$$

For N₂O-SP values, N₂O isotope mass contributions of BD, FD, and CD processes

to the total N_2O -SP_{NR} values production were expressed as:

$$N_2O - SP_{NR} = f_{BD} \times N_2O - SP_{BD} + f_{FD} \times N_2O - SP_{FD} + f_{CD} \times N_2O - SP_{CD} \quad (7)$$

where N_2O -SP_{NR} refers to the N_2O -SP value before reduction. N_2O -SP_{BD}, N_2O -SP_{FD}, and N_2O -SP_{CD} are the N_2O -SP values of BD (−7.5–3.7‰)^{65,76,84}, FD (27.2–39.9‰)^{75,76,85–87}, and CD (10–22‰)^{29,32,76,88}, respectively. Similarly, the contributions of the three endmembers to N_2O - $\delta^{18}O$ values of the three processes were expressed as:

$$N_2O - \delta^{18}O_{NR} = f_{BD} \times N_2O - \delta^{18}O_{BD} + f_{FD} \times N_2O - \delta^{18}O_{FD} + f_{CD} \times N_2O - \delta^{18}O_{CD} \quad (8)$$

where N_2O - $\delta^{18}O_{NR}$ refers to the N_2O - $\delta^{18}O$ value before reduction. N_2O - $\delta^{18}O_{BD}$, N_2O - $\delta^{18}O_{FD}$, and N_2O - $\delta^{18}O_{CD}$ are the N_2O - $\delta^{18}O$ values of BD (16.4–23.3‰)^{65,76,84}, FD (42.0–55.1‰)^{75,76,85–87}, and CD (24.9–37.6‰)^{29,32,76,88}, respectively.

Nitrogen and oxygen isotope fractionations during N_2O reduction such as BD can increase the measured N_2O -SP and N_2O - $\delta^{18}O$ values of remaining N_2O . Fractionation-derived shifts in N_2O -SP and N_2O - $\delta^{18}O$ values during N_2O reduction were thus estimated according to a previous study and presented as:

$$N_2O - SP = N_2O - SP_{NR} - f_R \times SP_{eN_2O} \quad (9)$$

$$N_2O - \delta^{18}O = N_2O - \delta^{18}O_{NR} - f_R \times \delta^{18}O_{eN_2O} \quad (10)$$

where SP and $\delta^{18}O$ are the N_2O -SP and N_2O - $\delta^{18}O$ values after N_2O reduction, respectively, which are the measured SP and $\delta^{18}O$ values here; f_R denotes the N_2O reduction ratio (0.75 in this study). This was estimated using the C_2H_2 approach⁴¹, i.e., the proportion of the residual (without C_2H_2 ; residual N_2O after N_2O reduction) to total (with C_2H_2 ; residual N_2O after N_2O reduction) N_2O concentrations. SP_{eN_2O} (−6‰) and $\delta^{18}O_{eN_2O}$ (−25‰) were assumed to be the fractionation effect during N_2O reduction^{76,89}. Given the N_2O reduction effect during experiments, Eqs. (7) and (8) were modified as:

$$N_2O - SP = f_{BD} \times N_2O - SP_{BD} + f_{FD} \times N_2O - SP_{FD} + f_{CD} \times N_2O - SP_{CD} - f_R \times SP_{eN_2O} \quad (11)$$

$$N_2O - \delta^{18}O = f_{BD} \times N_2O - \delta^{18}O_{BD} + f_{FD} \times N_2O - \delta^{18}O_{FD} + f_{CD} \times N_2O - \delta^{18}O_{CD} - f_R \times N_2O - \delta^{18}O_{eN_2O} \quad (12)$$

We further applied the Gaussian estimation and Monte Carlo sampling method to obtain the mean values and standard errors of N_2O -SP and N_2O - $\delta^{18}O$ for each endmember, and assess the errors of the mass balance model. The detailed MATLAB codes and Monte Carlo stimulations (10,000 sampling) are provided in Supplementary Table 2 and Supplementary Fig. 13. The values of SP and $\delta^{18}O$ -(N_2O/H_2O) used in the model for BD were −1.5‰ and 19‰, respectively; for FD were 37‰ and 47‰; for CD were 16‰ and 30‰. Combining Eqs. (6), (11), and (12), the relative contributions of BD, FD, and CD to N_2O productions are acquired in the plastisphere and bulk water. Proportions estimated by the equations are considered as zero if yielding negative values, and the other two proportions sum up to 100% accordingly.

D_2O -labeled single-cell Raman spectroscopy. To compare microbial phenotypic activity and to explore intracellular lipid/fatty acid levels between plastisphere and bulk water, a D_2O -labeled single-cell Raman spectroscopy experiment was performed^{15,90}. After the 30-d incubation, the four types of plastics were cut to produce $\sim 1.5 \times 1.5$ cm plastic fragments. For the plastisphere, 1 mL of sterilized bulk water and the plastic fragments were transferred to a 12-well plate and mixed with 1 mL D_2O , finally reaching a concentration of 50% D_2O . For bulk water, 1 mL of in situ bulk water and 1 mL D_2O were added to another 12-well plate. Each group was conducted in triplicate. The 12-well plates were anaerobically incubated at 300 rpm and 20 °C for 24 h. Next, plastic fragments were transferred to 5 mL phosphate buffer with 0.5% Tween-20, and attached microorganisms were separated by vortexing for 10 min. After washing with sterilized water twice (4000×g, 5 min), 2 μ L of microorganisms from bulk water and plastisphere were spotted on a tin foil-coated microslide and dried at 25 °C. Raman spectroscopy was acquired with a LabRAM Aramis (HORIBA Jobin-Yvon) confocal micro-Raman system, including a 300-g/mm diffraction grating, a 532-nm Nd:YAG laser, and a $\times 100$ objective (Olympus, Japan). We used the Raman characteristic band of a silicon wafer (520.6 cm^{-1}) to calibrate the Raman spectrometer. The generated spectra were subsequently analyzed in LabSpec-5 software (HORIBA Jobin-Yvon) with baseline correction and normalization. Peak intensities of Raman bands assigned to C–D (2040–2300 cm^{-1}) and C–H (2800–3100 cm^{-1}) were obtained to estimate (C–D)/(C–D + C–H) ratios⁴².

Denitrifier community. After the 24 h denitrification experiment, 2 mL of plastisphere suspension was taken for DNA extraction with a FastDNA Kit (MP, SA, USA). In situ bulk water samples were first filtered through sterilized 0.22 μ m polycarbonate filters that were then used for DNA extraction¹⁵. Bacterial *nirS* gene (*bnirS*-type denitrifier), bacterial *nirK* gene (*bnirK*-type denitrifier), and Internally

Transcribed Spacer (ITS) gene (fungal community) were used for amplicon sequencing with the primer sets (Supplementary Table 3). The obtained raw data were quality-filtered, chimera checked and then grouped at 97% similarity. Taxonomy was compared with GeneBank and UNITE databases using QIIME. Information of fungal *nirK* denitrifiers (*fnirK*-type denitrifiers) was screened from fungal communities based on previous studies and NR database^{36,91}. The coverage of screened operational taxonomic unit (OTU) to total OTUs of ITS data was >85%, which was used for subsequent analysis. The α -diversities including abundance-based coverage estimation (ACE), Chao1, Shannon, and Simpson indexes, were estimated in R. Principal coordinates analysis coupled with analysis of similarities (ANOSIM) test was applied to explore β -diversities of the three types of denitrifier communities. Co-occurrence network analysis was performed in R⁹² (nodes $R^2 > 0.90$ and $P < 0.05$) and visualized by Gephi (Version 0.9.2). Sequences will be submitted under accession number SUB10278422.

We investigated denitrifiers-based niche breadth and overlap according to Levins' niche breadth method and asymmetric α -model in R^{14,46,47}. These two indicators reflect the potential of denitrifiers adapting to environments and competing for resources in the plastisphere and bulk water. The formulas were as follow:

$$B_i = \frac{1}{\sum_{j=1}^N \times P_{ij}^2} \quad (13)$$

and

$$\alpha_{ij} = \frac{\sum_{i=1}^N \times P_{ia} \times P_{ja}}{\sum_{i=1}^N \times P_{ia}^2} \quad (14)$$

where B_i and α_{ij} are the niche breadth and overlap of denitrifier i in the plastisphere or bulk water, respectively; N denotes the total number of denitrifiers in each type of denitrifier community; P_{ij} denotes the proportion of denitrifier i in communities.

Gene abundance. The abundances of bacteria (16S rRNA) and fungi (ITS) in the plastisphere and bulk water were quantified with qPCR using the universal primers 515F/907R and ITS1F/ITS2R, respectively^{68,92}. The standard curves were obtained by a serial dilution of the plasmids with 16S rRNA and ITS genes. The mixing system (20 μ L) included 2 μ L of DNA sample, 10 μ L of Mix-enzyme (LightCycler SYBR Green I), 0.8 μ L of 515 F/907 R or ITS1F/ITS2R primers, and 7.2 μ L of H_2O . The thermal cycling conditions of 16S rRNA: 95 °C (3 min), 40 cycles at 95 °C (30 s), 55 °C (30 s) and 72 °C (45 s), and 72 °C (10 min). The thermal cycling conditions of ITS: 94 °C (10 min), 40 cycles at 94 °C (30 s), 56 °C (30 s) and 72 °C (45 s), and 72 °C (7 min). Samples with sterile pure water were regarded as negative control. Amplification efficiencies were 106.8–115.5% with $R^2 > 0.995$. Based on the Ribosomal RNA Operon Copy Number Database, microbial cell numbers could be assessed by the absolute abundances of 16S rRNA/4.1^{93,94}.

High-throughput qPCR-based SmartChip technique⁹⁵ was applied to detect denitrifying genes (*narG*, *nirS*, *nirK*, *nosZ*) abundances in the plastisphere and bulk water. The mixing system included 3.1 μ L of DNA sample, 24.8 μ L of Mix-enzyme (LightCycler SYBR Green I), and 3.1 μ L of denitrifying gene primers. They were dispensed into a SmartChip via a MultiSample NanoDispenser, and then quantified with a Real-Time PCR system (WaferGen, Biosystems, USA). The bacterial 16S rRNA (515 F/907 R) gene was set as a reference. The thermal cycle of qPCR conditions included heating at 95 °C (10 min), followed by 40 cycles at 95 °C (30 s), annealing at 58 °C (30 s), and extension at 72 °C (30 s). The threshold cycle of 31 was regarded as the detection limit. Information of primer pairs and other procedures are listed in our previous study⁹⁵ and Supplementary Table 4. Relative copy numbers of denitrifying gene and 16S rRNA gene were estimated as follows:

$$\text{Relative gene copy numbers} = 10^{(31 - \text{threshold cycle})} / (3.33) \quad (15)$$

Normalized relative denitrifying gene abundance was the proportion of the relative functional gene copy number to the 16S rRNA gene copy number.

Statistical analysis. In this study, the significance analyses on raw data were performed in IBM SPSS (Version 22.0). The significant differences in microbial activity, EPS concentration, c-di-GMP, and lipid/fatty acid level, N_2O concentration, denitrification rate, the proportion of denitrification pathways to N_2O production, functional gene abundance, denitrifiers-based niche breadth and overlap between plastisphere and bulk water were tested with one-way ANOVA method followed by a post-hoc Tukey test. P value < 0.05 was considered as significant.

Reporting summary. Further information on research design is available in the Nature Research Reporting Summary linked to this article.

Data availability

The sequence data generated in this study have been deposited in NCBI under accession NO. SUB10278422 (<https://www.ncbi.nlm.nih.gov>). The raw data of C–D ratios, lipids/fatty acids intensities, EPS, c-di-GMP, N_2O production, denitrification rate, percentage, isotope ratios, microbial communities generated in this study have been provided in the

Source Data file and also been uploaded in Dryad database <https://doi.org/10.5061/dryad.47d7wm3gz>. Other data are available in Supporting Information. Source data are provided with this paper.

Code availability

The codes of this study are available in Supporting Information.

Received: 27 October 2021; Accepted: 22 June 2022;

Published online: 06 July 2022

References

- Stubbins, A., Law, K. L., Munoz, S. E., Bianchi, T. S. & Zhu, L. Plastics in the Earth system. *Science* **373**, 51–55 (2021).
- Galloway, T. S., Cole, M. & Lewis, C. Interactions of microplastic debris throughout the marine ecosystem. *Nat. Ecol. Evol.* **1**, 1–8 (2017).
- Villarrubia-Gomez, P., Cornell, S. E. & Fabres, J. Marine plastic pollution as a planetary boundary threat—the drifting piece in the sustainability puzzle. *Mar. Policy* **96**, 213–220 (2018).
- Lopes, C., Raimundo, J., Caetano, M. & Garrido, S. Microplastic ingestion and diet composition of planktivorous fish. *Limnol. Oceanogr. Lett.* **5**, 103–112 (2020).
- Wright, S. L., Thompson, R. C. & Galloway, T. S. The physical impacts of microplastics on marine organisms: a review. *Environ. Pollut.* **178**, 483–492 (2013).
- Amelineau, F. et al. Microplastic pollution in the Greenland Sea: background levels and selective contamination of planktivorous diving seabirds. *Environ. Pollut.* **219**, 1131–1139 (2016).
- Nelms, S. E. et al. Plastic and marine turtles: a review and call for research. *ICES J. Mar. Sci.* **73**, 165–181 (2016).
- Seeley, M. E., Song, B., Passie, R. & Hale, R. C. Microplastics affect sedimentary microbial communities and nitrogen cycling. *Nat. Commun.* **11**, 1–10 (2020).
- Zettler, E. R., Mincer, T. J. & Amaral-Zettler, L. A. Life in the “Plastisphere”: microbial communities on plastic marine debris. *Environ. Sci. Technol.* **47**, 7137–7146 (2013).
- Amaral-Zettler, L. A., Zettler, E. R. & Mincer, T. J. Ecology of the plastisphere. *Nat. Rev. Microbiol.* **18**, 139–151 (2020).
- Wright, R. J., Erni-Cassola, G., Zadjelovic, V., Latva, M. & Christie-Oleza, J. A. Marine plastic debris: a new surface for microbial colonization. *Environ. Sci. Technol.* **54**, 11657–11672 (2020).
- Zhang, S.-J., Zeng, Y.-H., Zhu, J.-M., Cai, Z.-H. & Zhou, J. The structure and assembly mechanisms of plastisphere microbial community in natural marine environment. *J. Hazard. Mater.* **421**, 126780–126780 (2021).
- Dabrowska, A. A roadmap for a Plastisphere. *Mar. Pollut. Bull.* **167**, 112322 (2021).
- Li, C. et al. The ecology of the plastisphere: microbial composition, function, assembly, and network in the freshwater and seawater ecosystems. *Water Res.* **202**, 117428 (2021).
- Yang, K. et al. Temporal dynamics of antibiotic resistome in the plastisphere during microbial colonization. *Environ. Sci. Technol.* **54**, 11322–11332 (2020).
- Eric, W. & Mike, E. *Estuarine Ecohydrology*. 2nd edn, 322 (Elsevier Science, 2015).
- Lebreton, L. C. M. et al. River plastic emissions to the world’s oceans. *Nat. Commun.* **8**, 1–10 (2017).
- Kennish, M. J. & Townsend, A. R. Nutrient enrichment and estuarine Eutrophication. *Ecol. Appl.* **17**, S1–S2 (2007).
- Castro, P. & Freitas, H. *Linking Anthropogenic Activities and Eutrophication in Estuaries: The Need of Reliable Indicators* (Springer, 2011).
- Zumft, W. G. Cell biology and molecular basis of denitrification. *Microbiol. Mol. Bio. R* **61**, 533–616 (1997).
- Hou, L. J. et al. Effects of sulfamethazine on denitrification and the associated N₂O release in estuarine and coastal sediments. *Environ. Sci. Technol.* **49**, 326–333 (2015).
- Su, X., Chen, Y., Wang, Y., Yang, X. & He, Q. Impacts of chlorothalonil on denitrification and N₂O emission in riparian sediments: microbial metabolism mechanism. *Water Res.* **148**, 188–197 (2019).
- Thompson, R. L. et al. Acceleration of global N₂O emissions seen from two decades of atmospheric inversion. *Nat. Clim. Change* **9**, 993–+ (2019).
- Flemming, H.-C. et al. Biofilms: an emergent form of bacterial life. *Nat. Rev. Microbiol.* **14**, 563–575 (2016).
- Rumbaugh, K. P. & Sauer, K. Biofilm dispersion. *Nat. Rev. Microbiol.* **18**, 571–586 (2020).
- Su, X. X., Chen, Y., Wang, Y. Y., Yang, X. Y. & He, Q. Disturbances of electron production, transport and utilization caused by chlorothalonil are responsible for the deterioration of soil denitrification. *Soil Biol. Biochem.* **134**, 100–107 (2019).
- Thomson, A. J., Giannopoulos, G., Pretty, J., Baggs, E. M. & Richardson, D. J. Biological sources and sinks of nitrous oxide and strategies to mitigate emissions. *Philos. T. R. Soc. B* **367**, 1157–1168 (2012).
- Wankel, S. D. et al. Evidence for fungal and chemodenitrification based N₂O flux from nitrogen impacted coastal sediments. *Nat. Commun.* **8**, 1–11 (2017).
- Jones, L. C., Peters, B., Pacheco, J. S. L., Casciotti, K. L. & Fendorf, S. Stable isotopes and iron oxide mineral products as markers of chemodenitrification. *Environ. Sci. Technol.* **49**, 3444–3452 (2015).
- Maeda, K. et al. Relative contribution of nirK- and nirS- bacterial denitrifiers as well as fungal denitrifiers to nitrous oxide production from dairy manure compost. *Environ. Sci. Technol.* **51**, 14083–14091 (2017).
- Laughlin, R. J. & Stevens, R. J. Evidence for fungal dominance of denitrification and codenitrification in a grassland soil. *Soil Sci. Soc. Am. J.* **66**, 1540–1548 (2002).
- Wei, J., Ibraim, E., Bruggemann, N., Vereecken, H. & Mohn, J. First real-time isotopic characterisation of N₂O from chemodenitrification. *Geochim. Cosmochim. Acta* **267**, 17–32 (2019).
- Keusch, C. et al. NO and N₂O transformations of diverse fungi in hypoxia: evidence for anaerobic respiration only in *Fusarium* strains. *Environ. Microbiol.* **22**, 2182–2195 (2020).
- Shoun, H., Kim, D. H., Uchiyama, H. & Sugiyama, J. Denitrification by fungi. *FEMS Microbiol. Lett.* **94**, 277–281 (1992).
- Wang, L. et al. Bacterial and fungal assemblages and functions associated with biofilms differ between diverse types of plastic debris in a freshwater system. *Environ. Res.* **196**, 110371 (2021).
- Mothapo, N. et al. Phylogenetic, taxonomic and functional diversity of fungal denitrifiers and associated N₂O production efficacy. *Soil Biol. Biochem.* **83**, 160–175 (2015).
- Shoun, H., Fushinobu, S., Jiang, L., Kim, S. W. & Wakagi, T. Fungal denitrification and nitric oxide reductase cytochrome P450nor. *Philos. T. R. Soc. B* **367**, 1186–1194 (2012).
- Wang, M., Hu, R. G., Ruser, R., Schmidt, C. & Kappler, A. Role of chemodenitrification for N₂O emissions from nitrate reduction in rice paddy soils. *ACS Earth Space Chem* **4**, 122–132 (2020).
- Chen, D. et al. Chemodenitrification by Fe(II) and nitrite: pH effect, mineralization and kinetic modeling. *Chem. Geol.* **541**, 119586 (2020).
- Klueglein, N. & Kappler, A. Abiotic oxidation of Fe(II) by reactive nitrogen species in cultures of the nitrate-reducing Fe(II) oxidizer *Acidovorax* sp. BoFeN1—questioning the existence of enzymatic Fe(II) oxidation. *Geobiology* **11**, 396–396 (2013).
- Zou, Y. et al. Isotopomer analysis of nitrous oxide accumulated in soil cultivated with tea (*Camellia sinensis*) in Shizuoka, central Japan. *Soil Biol. Biochem.* **77**, 276–291 (2014).
- Ni, H. et al. Microbial metabolism and necromass mediated fertilization effect on soil organic carbon after long-term community incubation in different climates. *ISME J* **15**, 2561–2573 (2021).
- Hengge, R. Principles of c-di-GMP signalling in bacteria. *Nat. Rev. Microbiol.* **7**, 263–273 (2009).
- Davies, D. G. & Marques, C. N. H. A fatty acid messenger is responsible for inducing dispersion in microbial biofilms. *J. Bacteriol.* **191**, 1393–1403 (2009).
- Rabalais, N. N., Turner, R. E., Justic, D., Dortch, Q. & Wiseman, W. J. *Characterization of Hypoxia: Topic 1 Report for the Integrated Assessment on Hypoxia in the Gulf of Mexico* (NOAA Coastal Ocean Program Decision Analysis, 1999).
- Mo, Y. et al. Low shifts in salinity determined assembly processes and network stability of microeukaryotic plankton communities in a subtropical urban reservoir. *Microbiome* **9**, 128 (2021).
- Dezhi, L. et al. Models for niche breadth and niche overlap of species or populations. *Scientia Sinicae* **42**, 95–103 (2006).
- McDougald, D., Rice, S. A., Barraud, N., Steinberg, P. D. & Kjelleberg, S. Should we stay or should we go: mechanisms and ecological consequences for biofilm dispersal. *Nat. Rev. Microbiol.* **10**, 39–50 (2012).
- Hickman, J. W. & Harwood, C. S. Identification of FleQ from *Pseudomonas aeruginosa* as a c-di-GMP-responsive transcription factor. *Mol. Microbiol.* **69**, 376–389 (2008).
- Jenal, U., Reinders, A. & Lori, C. Cyclic di-GMP: second messenger extraordinaire. *Nat. Rev. Microbiol.* **15**, 271–284 (2017).
- Wolfe, A. J. V. & Visick, K. L. Get the message out: cyclic-di-GMP regulates multiple levels of flagellum-based motility. *J. Bacteriol.* **190**, 463–475 (2008).
- Marques, C. N. H., Davies, D. G. & Sauer, K. Control of biofilms with the fatty acid signaling molecule cis-2-decenoic acid. *Pharmaceuticals* **8**, 816–835 (2015).

53. Dow, J. M. et al. Biofilm dispersal in *Xanthomonas campestris* is controlled by cell-cell signaling and is required for full virulence to plants. *Proc. Natl Acad. Sci. USA* **100**, 10995–11000 (2003).
54. Virdis, B. et al. Biofilm stratification during simultaneous nitrification and denitrification (SND) at a biocathode. *Bioresour. Technol.* **102**, 334–341 (2011).
55. Kunming, X. U. Marine biofilm formation and its effect on metal corrosion. *Marine Sci.* **32**, 71–75 (2008).
56. Roager, L. & Sonnenschein, E. C. Bacterial candidates for colonization and degradation of marine plastic debris. *Environ. Sci. Technol.* **53**, 11636–11643 (2019).
57. Smith, C. S., Hinz, A., Bodenmiller, D., Larson, D. E. & Brun, Y. V. Identification of genes required for synthesis of the adhesive holdfast in *Caulobacter crescentus*. *J. Bacteriol.* **185**, 1432–1442 (2003).
58. Bonaglia, S. et al. Denitrification and DNRA at the Baltic Sea oxic-anoxic interface: substrate spectrum and kinetics. *Limnol. Oceanogr.* **61**, 1900–1915 (2016).
59. Tatariw, C., Chapman, E. L., Sponseller, R. A., Mortazavi, B. & Edmonds, J. W. Denitrification in a large river: consideration of geomorphic controls on microbial activity and community structure. *Ecology* **94**, 2249–2262 (2013).
60. Miao, Y. et al. Metagenomic insights into Cr(VI) effect on microbial communities and functional genes of an expanded granular sludge bed reactor treating high-nitrate wastewater. *Water Res.* **76**, 43–52 (2015).
61. Su, X. et al. Stimulation of N₂O emission via bacterial denitrification driven by acidification in estuarine sediments. *Glob. Change Biol.* **27**, 5564–5579 (2021).
62. Long, A., Heitman, J., Tobias, C., Phillips, R. & Song, B. Co-occurring Anammox, denitrification, and codenitrification in agricultural soils. *Appl. Environ. Microb.* **79**, 168–176 (2013).
63. Spott, O., Russow, R. & Stange, C. F. Formation of hybrid N₂O and hybrid N₂ due to codenitrification: first review of a barely considered process of microbially mediated N-nitrosation. *Soil Biol. Biochem.* **43**, 1995–2011 (2011).
64. Zhu-Barker, X., Cavazos, A. R., Ostrom, N. E., Horwath, W. R. & Glass, J. B. The importance of abiotic reactions for nitrous oxide production. *Biogeochemistry* **126**, 251–267 (2015).
65. Sutka, R. L. et al. Distinguishing nitrous oxide production from nitrification and denitrification on the basis of isotopomer abundances. *Appl. Environ. Microb.* **72**, 638–644 (2006).
66. Ouyang, L., Thamdrup, B. & Trimmer, M. Coupled nitrification and N₂ gas production as a cryptic process in oxic riverbeds. *Nat. Commun.* **12**, 1–8 (2021).
67. Stocker, T. F. et al. *Climate Change 2013: The Physical Science Basis. Contributions of Working Group I to the Fifth Assessment Report of the Intergovernmental Panel on Climate Change* (Cambridge University Press, 2013).
68. Su, X. et al. Bacterial communities are more sensitive to ocean acidification than fungal communities in estuarine sediments. *FEMS Microbiol. Ecol.* **97**, fiab058 (2021).
69. Cornejo-D'Ottone, M., Molina, V., Pavez, J. & Silva, N. Greenhouse gas cycling by the plastisphere: The sleeper issue of plastic pollution. *Chemosphere* **246**, 125709 (2020).
70. Purba, N. P. et al. Marine debris in Indonesia: a review of research and status. *Mar. Pollut. Bull.* **146**, 134–144 (2019).
71. Felz, S., Al-Zuhairy, S., Aarstad, O. A., van Loosdrecht, M. C. M. & Lin, Y. M. Extraction of structural extracellular polymeric substances from aerobic granular sludge. *J. Vis. Exp.* **115**, e54534 (2016).
72. Guo, Y. et al. Insight into c-di-GMP regulation in Anammox aggregation in response to alternating feed loadings. *Environ. Sci. Technol.* **51**, 9155–9164 (2017).
73. Spangler, C., Boehm, A., Jenal, U., Seifert, R. & Kaever, V. A liquid chromatography-coupled tandem mass spectrometry method for quantitation of cyclic di-guanosine monophosphate. *J. Microbiol. Met.* **81**, 226–231 (2010).
74. Thamdrup, B. & Dalsgaard, T. Production of N₂ through anaerobic ammonium oxidation coupled to nitrate reduction in marine sediments. *Appl. Environ. Microb.* **68**, 1312–1318 (2002).
75. Rohe, L., Well, R. & Lewicka-Szczepak, D. Use of oxygen isotopes to differentiate between nitrous oxide produced by fungi or bacteria during denitrification. *Rap. Commun. Mass Spectrom* **31**, 1297–1312 (2017).
76. Yu, L. et al. What can we learn from N₂O isotope data? Analytics, processes and modelling. *Rap. Commun. Mass Spectrom* **34**, e8858 (2020).
77. Yoshida, N. & Toyoda, S. Constraining the atmospheric N₂O budget from intramolecular site preference in N₂O isotopomers. *Nature* **405**, 330–334 (2000).
78. Coplen, T. B. Guidelines and recommended terms for expression of stable-isotope-ratio and gas-ratio measurement results. *Rap. Commun. Mass Spectrom* **25**, 2538–2560 (2011).
79. Lewicka-Szczepak, D. et al. Oxygen isotope fractionation during N₂O production by soil denitrification. *Biogeochemistry* **13**, 1129–1144 (2016).
80. Kool, D. M., Wrage, N., Oenema, O., Dolfing, J. & Van Groenigen, J. W. Oxygen exchange between (de) nitrification intermediates and H₂O and its implications for source determination of NO₃⁻ and N₂O: a review. *Rap. Commun. Mass Spectrom* **21**, 3569–3578 (2007).
81. Li Peiquan, K. X. The ratios of 18O/16O and its application in seawater. *Marine Sci.* **6**, 44–47 (1988).
82. Wang, Q. et al. Submarine groundwater discharge and associated nutrient fluxes in the Greater Bay Area, China revealed by radium and stable isotopes. *Geosci. Front.* **12**, 101223 (2021).
83. Lewicka-Szczepak, D., Augustin, J., Giesemann, A. & Well, R. Quantifying N₂O reduction to N₂ based on N₂O isotopocules—validation with independent methods (helium incubation and ¹⁵N gas flux method). *Biogeochemistry* **14**, 711–732 (2017).
84. Toyoda, S., Mutoke, H., Yamagishi, H., Yoshida, N. & Tanji, Y. Fractionation of N₂O isotopomers during production by denitrifier. *Soil Biol. Biochem.* **37**, 1535–1545 (2005).
85. Rohe, L. et al. Dual isotope and isotopomer signatures of nitrous oxide from fungal denitrification—a pure culture study. *Rap. Commun. Mass Spectrom* **28**, 1893–1903 (2014).
86. Sutka, R. L., Adams, G. C., Ostrom, N. E. & Ostrom, P. H. Isotopologue fractionation during N₂O production by fungal denitrification. *Rap. Commun. Mass Spectrom* **22**, 3989–3996 (2008).
87. Maeda, K. et al. N₂O production, a widespread trait in fungi. *Sci. Rep.* **5**, 1–7 (2015).
88. Stanton, C. L. et al. Nitrous oxide from chemodenitrification: a possible missing link in the Proterozoic greenhouse and the evolution of aerobic respiration. *Geobiology* **16**, 597–609 (2018).
89. Ostrom, N. E. et al. Isotopologue effects during N₂O reduction in soils and in pure cultures of denitrifiers. *J. Geophys. Res. Biogeosci.* **112**, 1–12 (2007).
90. Berry, D. et al. Tracking heavy water (D₂O) incorporation for identifying and sorting active microbial cells. *Proc. Natl. Acad. Sci. USA* **112**, E194–E203 (2015).
91. Mothapo, N. V., Chen, H., Cubeta, M. A. & Shi, W. Nitrous oxide producing activity of diverse fungi from distinct agroecosystems. *Soil Biol. Biochem.* **66**, 94–101 (2013).
92. Li, H. et al. Earthworms reduce the dissemination potential of antibiotic resistance genes by changing bacterial co-occurrence patterns in soil. *J. Hazard. Mater.* **426**, 128127 (2021).
93. Klappenbach, J. A., Saxman, P. R., Cole, J. R. & Schmidt, T. M. rrndb: the ribosomal RNA operon copy number database. *Nucleic Acids Res.* **29**, 181–184 (2001).
94. Zhu, D. et al. Antibiotics disturb the microbiome and decrease the incidence of resistance genes in the gut of a common soil collembolan. *Environ. Sci. Technol.* **52**, 3081–3090 (2018).
95. Zheng, B., Zhu, Y., Sardans, J., Penuelas, J. & Su, J. QMEC: a tool for high-throughput quantitative assessment of microbial functional potential in C, N, P, and S biogeochemical cycling. *Sci. China Life Sci.* **61**, 1451–1462 (2018).

Acknowledgements

We thank Prof. Xinping Chen for the constructive comments on this manuscript. This project was supported by the Natural Science Foundation of China (42003060, by Xiaoxuan Su), and Science Fund for Creative Research Groups of the National Natural Science Foundation of China (42021005, by Yong-guan Zhu).

Author contributions

X.X.S., L.Y.Y., Y.J.T., K.Y., J.L.P., H.L., and Y.-G.Z. conceived the study, designed and executed the incubations, analyzed the results, and wrote the manuscript. X.X.S. and Y.M.W. analyzed the community data. X.X.S. and L.Y.Y. measured N speciation. T.W. and H.L. detected N₂O isotopes. X.X.S. conducted single-cell Raman analysis. Y.J.T., L.R., Y.-G.Z., and M.R. edited the manuscript. All authors are involved in the interpretation of the results and the preparation of this manuscript.

Competing interests

The authors declare no competing interests.

Additional information

Supplementary information The online version contains supplementary material available at <https://doi.org/10.1038/s41467-022-31584-x>.

Correspondence and requests for materials should be addressed to Yong-guan Zhu.

Peer review information *Nature Communications* thanks Jian Liu, Tracy Mincer and Barth Smets for their contribution to the peer review of this work. Peer reviewer reports are available.

Reprints and permission information is available at <http://www.nature.com/reprints>

Publisher's note Springer Nature remains neutral with regard to jurisdictional claims in published maps and institutional affiliations.



Open Access This article is licensed under a Creative Commons Attribution 4.0 International License, which permits use, sharing, adaptation, distribution and reproduction in any medium or format, as long as you give appropriate credit to the original author(s) and the source, provide a link to the Creative Commons license, and indicate if changes were made. The images or other third party material in this article are included in the article's Creative Commons license, unless indicated otherwise in a credit line to the material. If material is not included in the article's Creative Commons license and your intended use is not permitted by statutory regulation or exceeds the permitted use, you will need to obtain permission directly from the copyright holder. To view a copy of this license, visit <http://creativecommons.org/licenses/by/4.0/>.

© The Author(s) 2022